The Effect of Impurity Concentration and Cr Content on the Passive Oxide Films in Ferritic Stainless Steels

Toshiaki Ohtsuka,[a,*,z] Masatoshi Abe,[a] and Tomohiro Ishii[b]

[a] *Faculty of Engineering, Hokkaido University, Kita-ku, Sapporo 060-8628, Japan*
[b] *Stainless Steel Research Department, Steel Research Laboratory, JFE Steel Corp., Chuo-ku, Chiba 260-0835, Japan*

The properties of passive oxides on three steels consisting of 11%Cr, 18%Cr, and 30%Cr-2%Mo were studied in acidic sulfate solution by the Mott-Schottky relation for semiconducting properties, potential modulation reflectance (PMR) spectroscopy for light absorption properties, X-ray photoelectron spectroscopy (XPS) for composition estimation, and Fe^{3+}/ Fe^{2+} redox current measurement for properties of electron transfer. The influence of the impurity concentration in the steels was also studied. The donor density in n-type semiconducting passive oxides as estimated from the Mott-Schottky plot decreased with a higher Cr content and with a lower impurity concentration. Cr enrichment occurred in the passive oxide and, for example, for 30Cr-2Mo steels, the ratio of Cr ions to total metallic ions in the passive oxide was approximately 70 wt%. The light absorption edge of the passive oxide measured by PMR was approximately 2.4 eV, irrespective of the Cr content and impurity concentration. The redox current on the passive oxide was much inhibited compared with that on the Pt electrode. The redox current decreased in a similar manner as the donor density. The inhibition of the redox current was assumed to be due to the space charge layer in the n-type semiconducting passive oxide.

 [DOI: 10.1149/2.0621510jes]

Manuscript submitted April 22, 2015; revised manuscript received July 23, 2015. Published August 1, 2015.

The non-metallic impurities in steels greatly affect the corrosion resistivity of the passive oxide film formed on them. The passive oxide usually covers the steels homogeneously and protects them against corrosion. When non-metallic deposits including impurities appear on the surface, the passive oxide irregularly covers the steels on the impurities, and the protection property of the passive oxide depends on the size and density of the surface deposits. Pitting corrosion may be initiated around the surface deposits. Muto et al. reported that surface deposits of manganese sulfide were initially dissolved by chloride-containing aqueous solution, and the pores or channels of the dissolved deposit worked as initiation sites of pitting corrosion.[1,2] Controlling the type and concentration of impurities may be one approach to achieve highly resistive passivated steels. Hara et al. noted that the thickness of the passive oxide on ferritic stainless steels decreased with a lower concentration of impurities.[3]

The passive oxide on iron has been proposed to possess an n-type semiconducting property that can be estimated from capacitance measurements and photo-electrochemistry.[4,5] The passive oxide on chromium has been reported to be p-type semiconducting[6] or to consist of both n-type and p-type semiconducting layers that are located in the inner and the outer parts of the passive oxide, respectively.[7] For the passive oxide on Fe-Cr ferritic stainless steel, an n-type semiconducting property was reported by Castro and Vilche.[8] Kim et al., however, reported a p-type semiconducting property for the passive oxide,[9] and Tsuchiya et al. proposed a hetero-junction consisting of the p-type semiconductor in the inner part of the passive oxide and the n-type in the outer part.[7,10,11] Fe-oxides such as Fe_2O_3 are represented as n-type semiconductors,[4,5] and Cr-oxides such as Cr_2O_3 are assumed to be p-type semiconductors. When one considers that the passive oxide on Fe-Cr ferritic steel consists of a mixture of both oxides, the properties of the passive oxide may depend on the mixture ratio of the two oxides.

For the element ratio of the passive oxide, ex situ X-ray photoelectron spectroscopy (XPS) has been widely applied. During the passivation in acidic solution, it has been reported that the Cr content was enriched in the passive oxide; for example, Asami et al. reported approximately 60% Cr content in the passive oxide on 18% Cr-Fe alloy.[12,13]

In this study, we prepared three ferritic steels of 11Cr-Fe, 18Cr-Fe, and 30Cr-2Mo-Fe with both conventional and extremely low levels of impurities. The effect of the impurities in the steels on the passive oxide formation in acidic sulfate solution was examined from using the electrochemical potential-current curve, the composition of the film as estimated by XPS, the donor density of the n-type semiconducting oxide as obtained by capacitance measurement, the light absorption property by potential modulation reflectance (PMR)[14,15] and the redox current of Fe^{3+}/Fe^{2+} through the passive oxide by redox current measurement in an aqueous solution containing Fe^{3+} and Fe^{2+} ions. From the measurement results, we discussed the band model of the oxide film and the effects of the impurities and Cr concentration in the alloys on the properties of the passive oxide film.

Experimental

In Tables I and II, the composition of the conventional steels and high purity steels of 11Cr-Fe, 18Cr-Fe, and 30Cr-2Mo-Fe is shown. In the high purity steels, the metallic elements of Cu, Ni, V, Nb, and Ti were present at less than detectable levels, while the other elements except for the basic elements of Cr, Fe, and Mo, as well as Al, were kept as low as possible. Commercial products were used for the conventional steels. The high purity steels were made as ingots in the Steel Research Laboratory, JFE Steel; rolled in sheets of 0.8-mm thickness; and annealed for 60 s at 1123 K for 11Cr and 18Cr steels and at 1223 K for 30Cr-2Mo steel. The steels were cut into disc form with a diameter of 15 mm. One side of the steel discs was polished by alumina abrasive of 0.05 μm diameter to achieve a mirror-like surface. The discs were pressed into a holder made of Teflon and sealed by Teflon spacer. The polished side was exposed to electrolyte solution with an exposure area of 0.785 cm^2, and the other side was contacted in the Teflon holder to a brass disc that was connected by a copper wire to a potentiostat.

A H-500 potentiostat by Hokuto Denko was used for electrochemical measurements. For capacitance measurements to estimate the semiconducting property of the passive oxide by the Mott-Schottky equation, the AC impedance was measured by a frequency response analyzer, an NF Design Circuit 5020 connected to a potentiostat made in our laboratory. For the AC impedance, an AC amplitude at 0.01 V_{rms} was applied through the potentiostat to the steel electrode at a frequency of 13 Hz. A mixture containing 0.01 mol H_2SO_4 and 0.09 mol Na_2SO_4 per 1 dm^3 solution (0.01 M H_2SO_4-0.09 M Na_2SO_4 solution) at pH 2.25 were used for the passivation study.

The redox current of Fe^{3+}/Fe^{2+} on the passivated steels was measured in an acidic solution of 0.01 M H_2SO_4-0.09 M Na_2SO_4

*Electrochemical Society Active Member.
[z]E-mail: ohtsuka@eng.hokudai.ac.jp

Table I. Composition in wt% of commercial steels.

Steel	C	Si	Mn	P	S	Cr	Mo	N	Nb	Ti	Fe
11Cr	0.008	0.28	0.41	0.024	0.001	11.0	–	0.007	–	0.24	Bal
18Cr	0.007	0.19	0.26	0.031	0.001	17.5	–	0.012	–	0.28	Bal
30Cr-2Mo	0.005	0.18	0.11	0.026	0.007	29.9	1.91	0.012	0.13	–	Bal

Table II. Composition in wt% of high-purity steels.

Steel	C	Si	Mn	P	S	Cr	Mo	N	Fe
11Cr	0.0010	0.009	0.010	0.008	<0.0007	11.0	–	0.0012	Bal
18Cr	0.0020	0.022	0.002	0.005	<0.0007	18.0	–	0.0020	Bal
30Cr-2Mo	0.0015	0.026	0.001	0.005	<0.0007	29.8	1.87	0.0025	Bal

containing $(NH_4)_2Fe(SO_4)_2$ at a concentration of 0.05 mol dm^{-3} (M) and $NH_4Fe(SO_4)_2$ at 0.05 M.

For the electrochemical measurements, a glass cell with 200 mL solution was used, equipped with a counter electrode of platinum sheet and a Luggin glass capillary connected to a reference electrode of Ag/AgCl/saturated KCl (SSC).

The potential modulation reflectance (PMR) spectroscopy was measured by an apparatus reported in previous papers.[14,15] The passivation of the steels was done at 0.6 V for 1 h, followed by the PMR measurement at the same potential. The frequency of the potential modulation was 13 Hz, and the measurement spectrum ranged between the 300 nm and 700 nm wavelengths of light, with the PMR taken at 20 nm intervals.

For the estimation of the oxide composition on the steels, X-ray photoelectron spectroscopy (XPS) was used (JEOL JPS-9200). After 1 h of passivation at 0.6 V in 0.01 M H_2SO_4-0.09 M Na_2SO_4 solution, the steel disc was removed from the Teflon holder, washed in pure water, and dried. The steel disc was quickly stored in a dry box filled with N_2 gas and then transferred to the XPS apparatus. The XPS measurement of the steel disc was started as soon as possible. The XPS measurement was made by an MgKα X-ray source at 1253.6 eV. The calibration of the binding energy of the photoelectron was done with the signal of Au4f7/2 at a binding energy of 84.00 eV.

Results

Potential-current relation.— The potential (E)-current density (CD, i) relation was measured in 0.01 M H_2SO_4-0.09 M Na_2SO_4 mixture solution at pH 2.25 by a potential sweep from −0.7 V to 1.5 V at a rate of 2×10^{-4} V s^{-1}. Fig. 1 shows the E-i relation for 11Cr steels. A large active region is seen from −0.62 V to 0.1 V vs. Ag/ AgCl/ saturated KCl (SSC), followed by a passive region. The transpassive region starts at 0.8 V, and oxygen evolution was seen from 1.4 V. A large difference between the conventional and high-purity 11Cr steels is not seen, except for a larger active peak of the high purity steel at approximately −0.35 V.

The E-i relation for the 18Cr steels is shown in Fig. 2, in which a negative loop is seen. In Fig. 2B, an expanded linear plot of i vs. E is shown in which the negative CD region (i.e., negative loop) was observed from −0.46 V to −0.40 V, following the active region. The passive region was expanded to between −0.35 V and 0.8 V. The

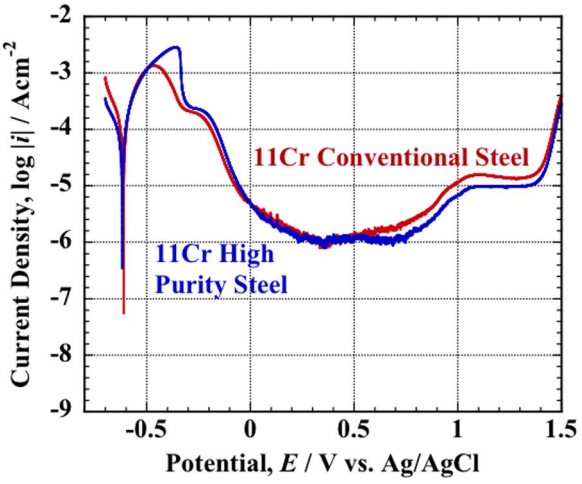

Figure 1. Potentiodynamic Potential-current curve of 11Cr conventional and high purity steels in 0.01 M H_2SO_4-0.09 M Na_2SO_4 mixture solution at pH 2.25. The potential sweep rate was 2×10^{-4} V s^{-1}.

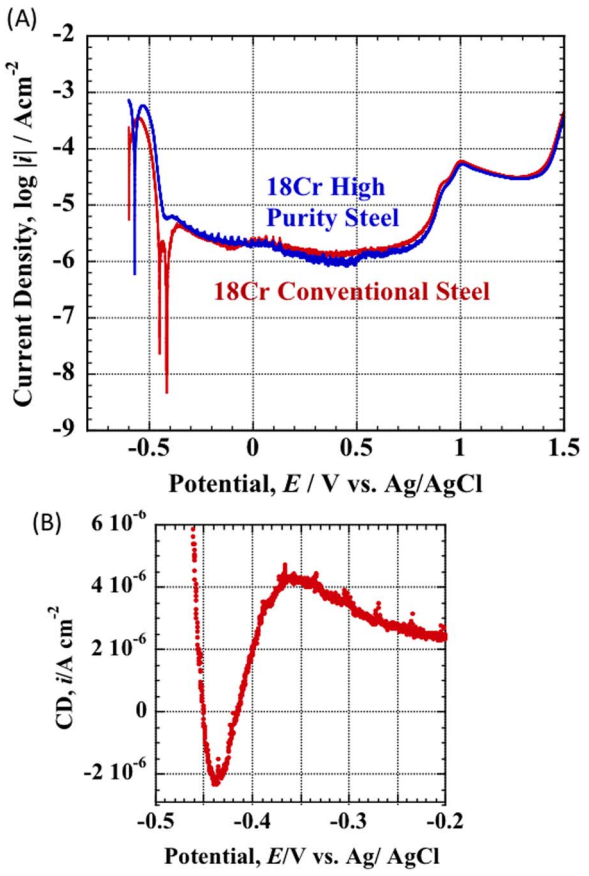

Figure 2. (A) Potentiodynamic Potential-current curve of 18Cr conventional and high purity steels in 0.01 M H_2SO_4-0.09 M Na_2SO_4 mixture solution at pH 2.25. The potential sweep rate was 2×10^{-4} V s^{-1}. (B) Negative loop of 18Cr conventional steel at the initial of passive region.

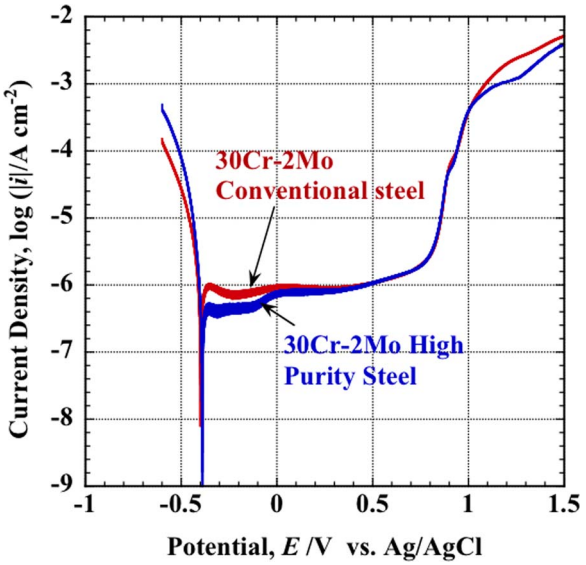

Figure 3. Potentiodynamic Potential-current curve of 30Cr-2Mo conventional and high purity steels in 0.01 M H_2SO_4-0.09 M Na_2SO_4 mixture solution at pH 2.25. The potential sweep rate was 2×10^{-4} V s^{-1}.

transpassive and oxygen evolution regions started from 0.8 V and 1.4 V, respectively, similar to the values for the 11Cr steels.

The similar *E-i* relation for the 30Cr-2Mo steels is shown in Fig. 3, in which a very small active region is seen at approximately −0.4 V and the passive region extends from −0.35 V to 0.8 V. The passive current of the high-purity steel was slightly smaller than that of the conventional steel at potentials lower than 0.0 V. The transpassive region started at 0.8 V, and the oxygen evolution was not clearly seen due to the large transpassive current.

The negative loop is notably observed only in the conventional 18Cr steel at approximately −0.43 V. The negative loop was often observed on stainless steels between the active and the passive regions, when the cathodic current density (CD) of the hydrogen evolution reaction (HER) exceeds the anodic passive CD at the beginning of the passive region. For the 11Cr steel, because the anodic active CD is much larger than the cathodic CD of the HER at approximately −0.43 V, the negative loop cannot be seen, and for the 30Cr-2Mo steel because the active CD is low and the active potential region is small, the cathodic CD of the HER appears at a potential region of approximately −0.43 V. For high-purity 18Cr steel, the cathodic CD of HER may be smaller than that for the conventional 18Cr steel because of the smaller amount of surface impurity precipitate, which can work as active points of the HER, and thus no negative loop may appear.

XPS spectra of the passivated steels.— For the estimation of composition ratio of Fe, Cr, and Mo in the passive oxide film, XPS spectra were measured. Figures 4 and 5 show the spectra of Fe 2p(3/2) and Cr 2p(3/2), respectively, for the three high-purity steels passivated at 0.6 V vs. SSC for 1 h. For the conventional steels, almost the same XPS spectra were measured, as shown in Figs. 4 and 5. In Fig. 4, the spectrum of Fe 2p(3/2) was decomposed into two chemical states, one metallic Fe at a peak binding energy (BE) of 706.8 eV and the other oxidized Fe at a BE of 710.9 eV. Though several authors have further deconvoluted the oxidized Fe spectrum into a few chemical states,[16–18] we treated the oxidized Fe spectrum as an element with a relatively large half width. The peak energy of the oxidized Fe spectrum corresponds to that of the Fe^{3+} state in the oxide. The relative intensities of the oxidized Fe spectrum to the metallic Fe was in the order of 30Cr-2Mo steel < 18Cr steel < 11Cr steel, and thus the film thickness was assumed to increase with the order because the signal intensity of the metallic Fe is attenuated more with the thicker oxide

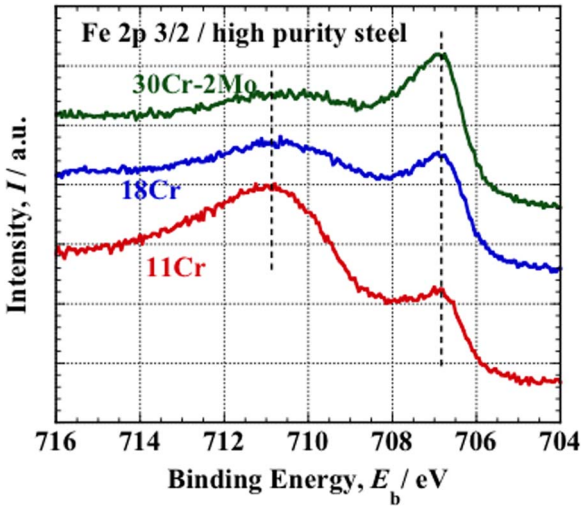

Figure 4. Fe 2p 3/2 XPS spectra of passive oxide anodically formed on high purity steels.

film. The change in the relative intensity between the conventional and high-purity steels was not clearly seen.

In Fig. 5, the spectrum of Cr 2p(3/2) can also be deconvoluted to metallic Cr at 574.1 eV BE and oxidized Cr at 576.8 eV. The peak energy of the oxidized Cr corresponds to that of Cr^{3+}.[16–18] The relative intensities of the oxidized Cr spectrum to the metallic Cr is in the order of 30Cr-2Mo steel < 18Cr steel < 11Cr steel, similar to the Fe spectra.

In Fig. 6, the spectra of Mo 3d(3/2) and 3d(5/2) are shown for 30Cr-2Mo steels passivated at 0.6 V for 1 h. The intensity of Mo is much weaker than those of Fe and Cr, proportional to the lower concentrations of Mo in the steels.

The oxygen spectra (O 1s) of the passivated steels were also measured by XPS. The results are shown in Fig. 7 for the high-purity steels. For the conventional steels, similar XPS spectra were measured. The spectra can be deconvoluted into two signals. The higher peak at 530.2 and the lower peak at 532.1 eV are assumed to correspond to the O^{2-} state and OH^- state in the passive oxide, respectively. The relative intensity of the OH^- signal to the O^{2-} signal increases with the higher Cr concentration in the steels. Because it is assumed that the thickness decreases with an increase in the Cr concentration, as shown in Figs. 4 and 5, and OH- mainly occupies the outer hydrated part in the passive

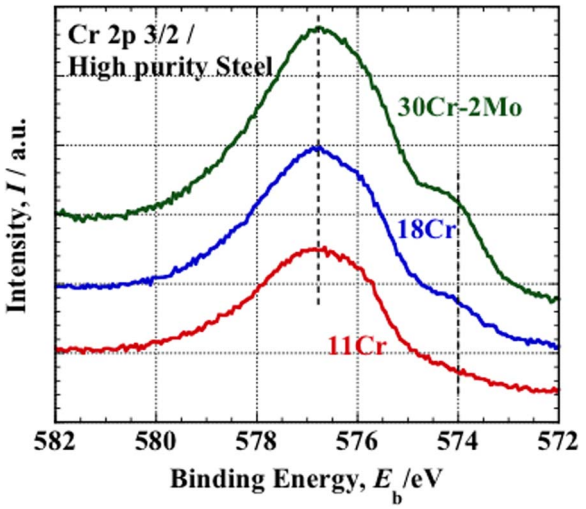

Figure 5. Cr 2p 3/2 XPS spectra of passive oxide anodically formed on high purity steels.

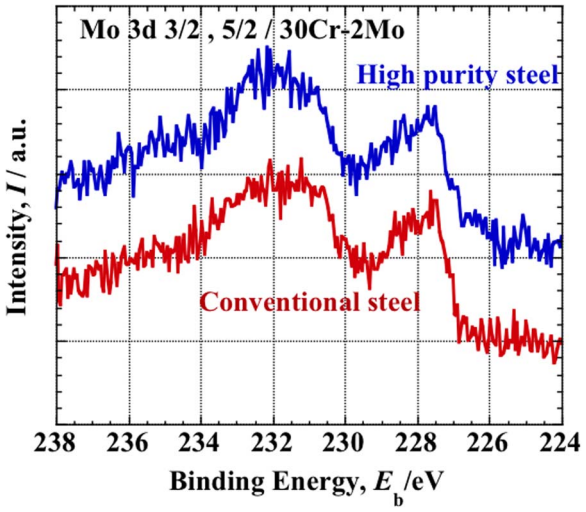

Figure 6. Mo 3d 3/2 and 5/2 XPS spectra of passive oxide anodically formed on 30Cr-2Mo conventional and high purity steels.

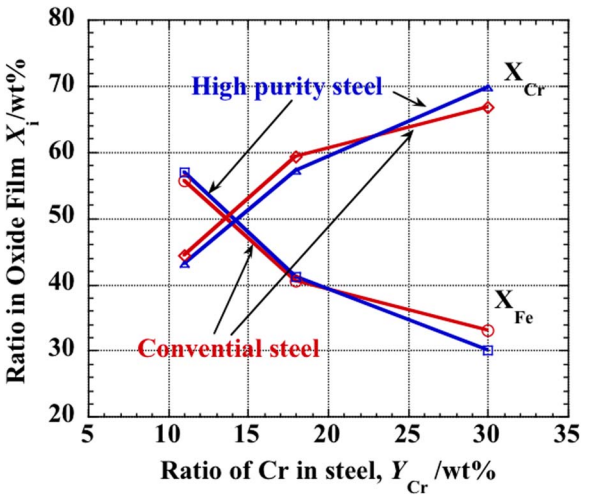

Figure 8. Concentration ratios of Fe and Cr in the oxide film anodically formed at 0.6 V vs. Ag/ AgCl in acidic sulfate solution at pH 2.25 as a function of the ratio of Cr in the steels.

oxide,[13,18] the thickness of the inner dehydrated part can be estimated to decrease with an increase in the Cr concentration.

The concentration ratio of Cr and Fe in the passive oxide was calculated by the relative intensities of the XPS signals shown in Figs. 4 and 5. The calibration from the relative intensities of XPS signals to the concentration ratio of Cr to Fe was made by a comparison between the intensities for the bare steels and the bulk concentrations in the steels. The intensities of the bare steel were measured after Ar ion sputtering of the steel surface for approximately 10 min, at which point no oxygen signal was detected. Fig. 8 shows the mass ratio thus calculated of Fe (X_{Fe}) and Cr (X_{Cr}) in the passive oxide as a function of the concentration of Cr in the steels. For 30Cr-2Mo steel, the small concentration of Mo in the passive oxide was neglected. The Cr content in the passive film is seen to be enriched compared with the bulk concentration of Cr in the steel; for the 11Cr, 18Cr, and 30Cr-2Mo steels, the Cr content is enriched by four, three, and two-and-a-half times relative to the bulk concentration of steels, respectively. The difference between high-purity and conventional steels is not clearly seen in the enrichment factors.

Spectra of potential modulation reflectance (PMR).— To survey the spectroscopic optical properties of the passive oxide on the steels, the PMR was measured as a function of the wavelength of light between 300 and 700 nm. The results for the high-purity steels are shown in Fig. 9, in which the data of the three steels of 11Cr, 18Cr, and 30Cr-2Mo are plotted. The steels were passivated at 0.6 V vs. SSC for 1 h before the PMR measurement at the same potential. In Fig. 9, no distinct difference among the three steels was seen in the scatter of the measured data. For the conventional steels, PMR measurements obtained almost the same results.

In Fig. 9, one can see a threshold wavelength of light at 500 nm. For wavelengths shorter than 500 nm, the PMR increases, and for wavelengths longer than 500 nm, the PMR remains almost constant. The threshold wavelength may be the light-absorption edge, as previously reported on passive oxides on SUS304 stainless steel[14] and pure Fe.[15]

Mott-Schottky plot of the capacitance.— The *E-i* relation, composition of the passive oxide by XPS and spectroscopic property by

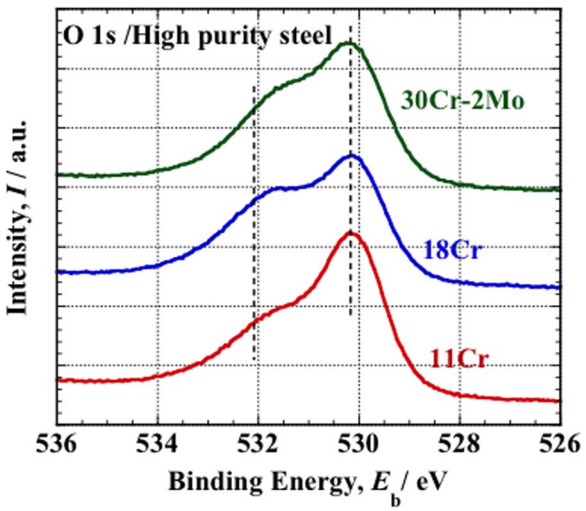

Figure 7. O1s XPS spectra of passive oxide anodically on high purity steels.

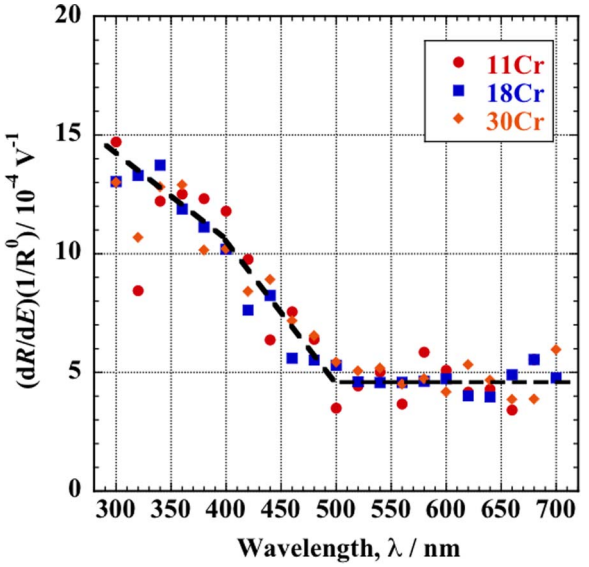

Figure 9. Spectra of potential modulation reflectance (PMR) of the high-purity steels of 11Cr, 18Cr, and 30Cr-Mo passivated at 0,6 V for 1 h in 0.01M H_2SO_4 and 0.09 M Na_2SO_4. The PMR was measured at the same potential after the passivation.

PMR depends on the Cr concentration of the steels but not on the impurity concentration. The average properties mentioned above may be insensitive to the impurities. The semiconducting property of the passive oxide is assumed to be greatly influenced by localized defects in the passive oxide, and the impurity surface deposits are expected to provide the defect sites in the oxide. Thus, the semiconducting property should change with the impurity concentration.

For the semiconducting property of the passive oxide formed at 0.6 V for 1 h, the capacitance was measured at a frequency of $f = 13$ Hz as a function of the potential, which was decreased stepwise from the formation potential of 0.6 V to −0.3 V by a step of 0.02 V and a step interval of 10 s. The capacitance was assumed to correspond to that of the dielectric layer that was formed as a space charge layer in the semiconducting passive oxide. The capacitance was estimated from the imaginary part of the AC impedance ($Z = X - jY$).

$$C = 1/(2\pi f Y)$$

For the selection of the frequency, we first measured the impedance spectra of the stainless steels at frequencies from 0.01 Hz to 20 kHz at 0.6 V, the same as that for the passivation. The phase shifts of the impedance exhibited a maximum in the negative direction at about −75 degrees for frequencies of 1–30 Hz.[14] At these frequencies, the impedance was more occupied by the capacitance than the film resistance and ohmic solution resistance that were connected in parallel with the capacitance and in series with the parallel circuit consisting of the capacitance and the film resistance, respectively. The frequency of 13 Hz in the middle of the above frequency region was adopted to measure the capacitance. Because the capacitance of the space charge layer, C_{SC}, is assumed to be connected in series with the capacitance of the electric double layer, C_{DL}, on the oxide surface, the contribution of C_{DL} should be subtracted from the capacitance measured.

$$1/C_{SC} = (1/C) - (1/C_{DL})$$

The exact values of C_{DL} on the oxide surface have not been reported. If the C_{DL} is large enough, for example, larger than 10^{-4} F cm^{-2}, the contribution of C_{DL} to the C measured becomes negligibly small.

In Fig. 10, the capacitance measured for the steels passivated at 0.60 V vs. SSC is plotted as C^{-2} vs. E according to the Mott-Schottky equation for n-type semiconductors without the subtraction of C_{DL}.

$$C^{-2} = (2/eN_D\varepsilon\varepsilon_0)[E - E_{FB} - (kT/e)]$$

where E_{FB} is the flatband potential, N_D the donor density, ε the dielectric constant of the oxide, ε_0 the permittivity of vacuum, k the Boltzmann constant, and T the temperature. From the plot, the positive slope of C^{-2} vs. E indicates that the oxide film behaves as an n-type semiconducting layer. In Fig. 10, one can evaluate the N_D and E_{FB} from the slope and the intercept on the potential axis, respectively. N_D thus evaluated with an assumption of the dielectric constant of the oxide $\varepsilon = 12$ was plotted as a function of the Cr concentration of the steels in Fig. 11. For both the 11Cr steels and the 18Cr steels, N_D of the high-purity steels is smaller than that of the conventional steels, but for the 30Cr-2Mo steels, N_D had almost the same value.

The flatband potential E_{FB} estimated from the intercept on the potential axis in Fig. 10 shifts to a lower potential at a higher concentration of Cr.

Fe^{3+}/Fe^{2+} redox current through the passive oxide.— The rate of electron transfer between the steel and redox couple in the electrolyte changed with the property of the passive oxide. When a space charge layer or depletion layer is present in the passive oxide, it works as a barrier and inhibits the electron transfer rate of the redox couple. The inhibition was verified from the current density (CD) of the Fe^{3+}/Fe^{2+} redox couple on the passive oxide.[19]

Figure 12 shows the CD of Fe^{3+}/Fe^{2+} redox couple on the passive oxide formed at 0.6 V on the 18Cr steels. The measurement was performed by a potential sweep from 0.6 V to −0.4 V at a sweep rate of 2×10^{-3} V s^{-1}.

$$Fe^{3+} + e^- \rightleftarrows Fe^{2+}$$

The CD on the Pt electrode is shown as a comparison in Fig. 12. On the Pt electrode, the CD reaches a diffusion-controlled CD with a small polarization in both the anodic and cathodic directions. The exchange

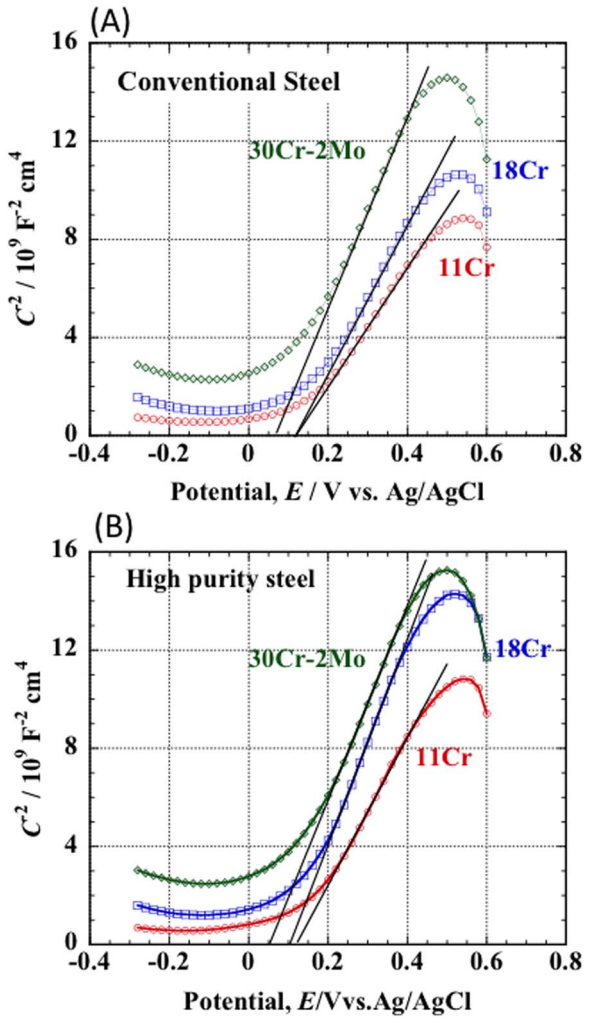

Figure 10. Mott-Schottky plot of capacitance for 11Cr, 18Cr, 30Cr-2Mo steels. (A) Conventional steels and (B) high purity steels.

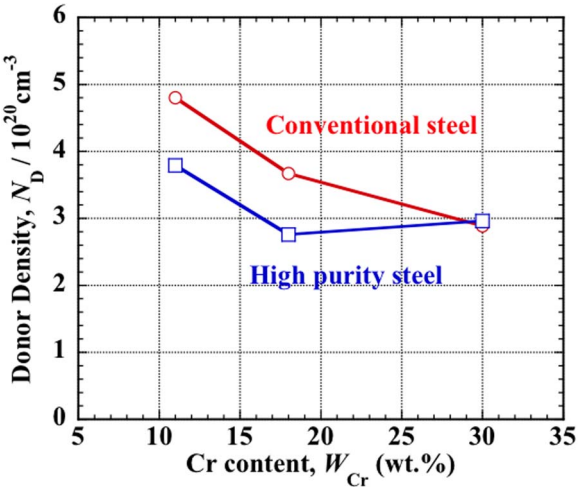

Figure 11. Donor density in the passive oxide anodically formed at 0.60 V as a function of ratio of Cr in the steels.

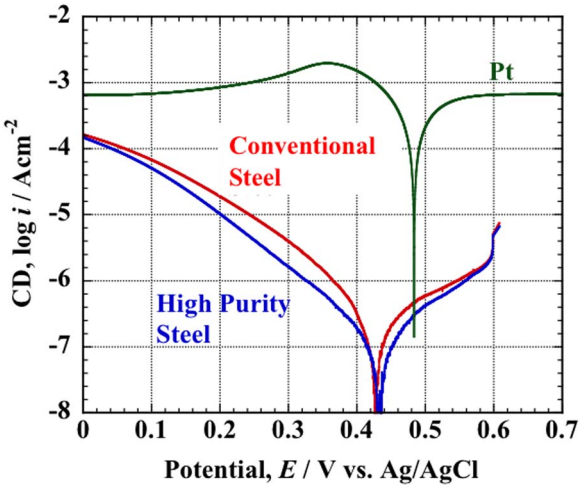

Figure 12. Fe^{3+}/Fe^{2+} redox CD on 18Cr steels covered with passive oxide film. The redox CD on Pt electrode was plotted for the comparison.

CD on the Pt electrode may be three orders higher than that of the 18Cr steels covered by the passive oxide. When comparing the CDs of the high-purity steel and the conventional steel, the CD of the conventional steel is slightly higher. The potentials at zero current are significantly different between the Pt electrode and the steel electrodes: 0.483 V vs. SSC for the Pt electrode, 0.433 (±0.0015) V for the high-purity steels, and 0.428 (± 0.0015) V for the conventional steels. The zero-current potential on the Pt electrode is probably coincident with the equilibrium potential of Fe^{3+}/Fe^{2+} at a concentration of 0.05 M. The negative shift of the zero-current potential on the steels covered by the oxide from the potential on Pt indicates that the cathodic CD was more inhibited by the barrier of the passive oxide. The small difference in the zero-current potential between the high-purity and conventional steels was not adequately explained, and we assumed that the difference is large than an artifact error.

For a quantitative comparison among the exchange currents, we calculated the linear polarization resistance from the *E-i* plot in the neighborhood of the zero-current potential. From the plot, the resistance $R_p = dE/di$ was calculated. In Fig. 13, the polarization resistances thus calculated are shown as a functions of the ratio of Cr in the steels. The resistances are approximately 10^5 Ω cm^{-2} in the order

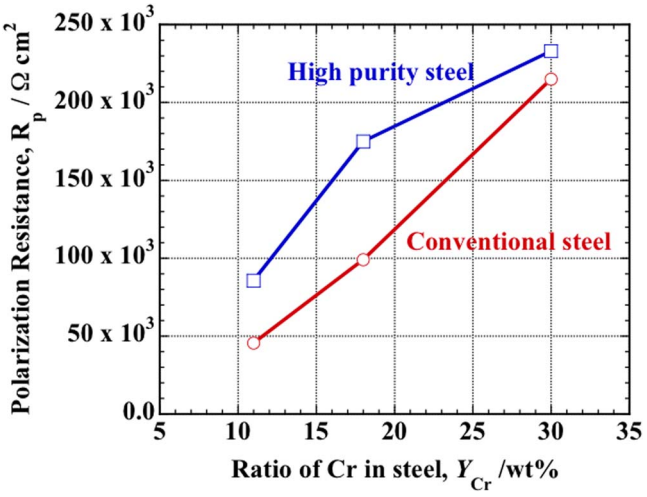

Figure 13. Polarization resistance for Fe^{3+}/Fe^{2+} redox reaction on steels covered with passive oxide film formed at 0.60 V as a function of ratio of Cr in the steels.

of 30Cr-2Mo > 18Cr > 11Cr, and three orders larger than that of the Pt electrode, $R_p = 75$ Ω cm.[2] From Fig. 13, it is seen that R_p increases with a higher Cr content in the steels and a lower impurity concentration.

From the polarization resistance one can estimate the exchange CD (i_0) of the Fe^{3+}/Fe^{2+} redox reaction from the following equation.

$$i_0 = \left(1/2.303R_p\right)\left(1/\beta_a + 1/\beta_c\right)^{-1}$$

where β_a is the anodic Tafel slope and β_c the cathodic Tafel slope for the redox reaction. The exchange CD thus calculated from the resistance and the Tafel slopes is plotted in Fig. 14 as a function of the ratio of Cr in the steels. The increase in Cr content in the steels reduces the Fe^{3+}/Fe^{2+} redox CD. For the 11Cr and 18Cr steels, the exchange CDs of the high-purity steel are twice as large as those of the conventional steel. For the 30Cr-2Mo steels, the difference is not as large, although the exchange CDs are much smaller than those for the 11Cr and 18Cr steels.

Discussion

Critical Cr concentration of stainless steels.— Stainless steels include Cr at ratios higher than the critical concentration of 13%. When one compares the active dissolution regions of the 11Cr and 18Cr steels, the maximum CD of the 11Cr steel is one order higher than that of the 18Cr steel, and the active potential region of the 11Cr steel is much wider than that of the 18Cr steel. When the 11Cr steel is immersed in an aerated neutral pH or slightly acidic solution, spontaneous passivation may be difficult to achieve due to the large width of the active region, in contrast with the 18Cr steel, which may be spontaneously passivated and maintains its passive state. The Cr ratio in the passive oxide film, as shown in Fig. 8, was approximately 43–45% for the 11Cr steel and 57–60% for the 18Cr steel. We believe that the lowest Cr ratio in the passive oxide required for maintaining the passive state for a long time period may be approximately 50%, and 13% Cr, which is a critical concentration for stainless steels, is required in the substrate alloy to form the passive oxide, including the Cr at a 50% ratio.

Property of passive oxide depending on the Cr content of the steels.— The donor density N_D and the current density (CD) of the Fe^{3+}/Fe^{2+} redox couple were a function of Cr ratio in the steels, both decreasing with the increase of the Cr ratio. In the passive oxide, Cr is enriched in the oxide film compared with Cr in the substrate steels. From the relative intensity of the XPS spectra of Fe^0/Fe^{3+} and Cr^0/Cr^{3+}, as shown in Figs. 4 and 5, the oxide films are assumed to become thinner with an increase of Cr in the substrate steel.[12,13,18] The influence of the Cr content is summarized as follows. When the Cr content in the substrate steel is increased, (1) Cr enrichment in the oxide film is enhanced, (2) the thickness of the passive film becomes smaller, (3) N_D in the oxide film is decreased, and (4) the Fe^{3+}/Fe^{2+} redox current on the oxide film is decreased.

We believe that the enrichment of the Cr content in the oxide film is the largest factor to occupy the property of the passive oxide layer. For 30Cr-2Mo steel, although the thickness of the passive oxide layer with a higher enrichment of Cr is smaller than that of the steels of lower Cr, the barrier of the oxide against electron transfer works more effectively. The barrier efficiency will be discussed in connection with the donor density in the section of model of electron transfer on n-type semiconducting passive oxide.

Influence of impurity concentration on the passive oxide.— The composition of the passive oxide did not depend on the impurity concentration, as shown in Fig. 8, in which the enrichment of Cr in the oxide film did not change between the conventional and high-purity steels. When the impurity concentration in the steels decreased, however, the donor density N_D in the passive oxide decreased, as shown in Fig. 10, and the redox current of Fe^{3+}/Fe^{2+} is also decreased, as shown in Fig. 14. The average properties of the composition, thickness, and light absorption of the passive oxide are not significantly

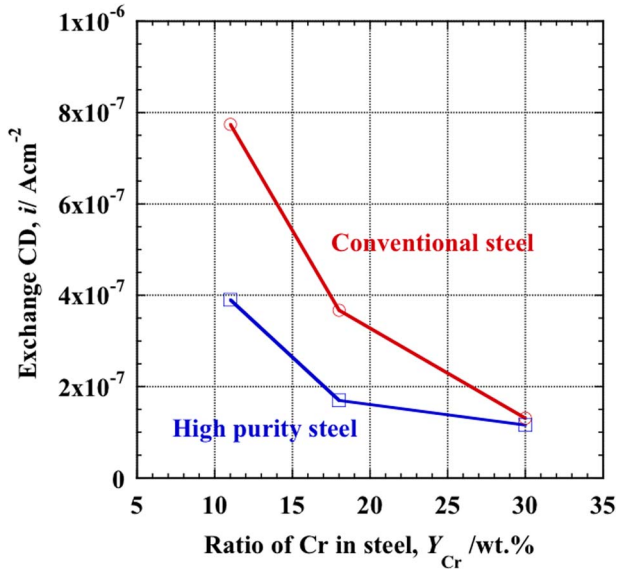

Figure 14. Exchange CD for Fe^{3+}/Fe^{2+} redox reaction on steels covered with passive oxide film formed at 0.60 V as a function of ratio of Cr in the steels.

influenced by the impurity concentration. When the impurities of the steels appear on the surface as deposits of non-metallic compounds, however, the passive oxide layer on the deposit or in the vicinity of the deposit may be influenced, and heterogeneity is induced in the passive oxide layer. Consequently, the oxide layer includes defects on the deposits or in the vicinity of the deposit. The defect sites work as electron donors and accelerate the electron transfer. In addition, the defect sites possibly work as initiation sites of localized corrosion like pitting corrosion and SCC. It may be concluded that the steels with lower impurity concentrations are covered by a better quality passive oxide film with a smaller number of defect sites.

Model of electron transfer on n-type semiconducting passive oxide.— When one considers the flatband potential (E_{FB} = 0.080 V vs. SSC) for the 18Cr steels from the Mott-Schottky plot in Fig. 10 and the Fe^{3+}/Fe^{2+} redox potential (E_{Redox} = 0.482 V vs. SSC)) in Fig. 12, one can draw a model of potential distribution at specified electrode potentials for the 18Cr steel. The model is shown in Fig. 15A at E = 0.482 V, where the Fermi level (ε_F) of the steel was fixed at the redox electron potential (ε_{Redox}), i.e., the potential difference appearing in the oxide film, $\Delta E = E_{Redox} - E_{FB}$. The edge of the conduction band curves in the upper direction to the oxide film/ electrolyte interface, and thus the space charge layer is formed, where the positively ionized donors are fixed and few carriers exist. On the electrolyte side, the densities of state on the logarithmic scale for the occupied state D_{oc} for Fe^{2+} and for the unoccupied state D_{un} for Fe^{3+} were schematically drawn. An absence of carriers, i.e., an absence of free electrons, in the surface space charge layer means that the layer works as barrier against electron transfer between the inner side of the oxide and the redox species in the electrolyte.

$$Fe^{3+}{}_{(el)} + e_{(CB)} \rightleftarrows Fe^{2+}{}_{(el)}$$

where the transfer rate (r) of the reduction reaction may be proportional to the concentration of electrons $n_{(CB)}$ at the lower edge of the conduction band in the inner oxide film and the density of state for the unoccupied state D_{un} at the energy level of the conduction band edge.

$$r = kn_{(CB)}D_{un}$$

The rate constant (k) includes a probability of electrons tunneling through the surface barrier. From comparison of the exchange CD on the steels with the CD on Pt, the barrier effect is expected to be 10^3. The electrons tunnel from the inner side of the oxide film to the redox species in the electrolyte through two possible routes: One is the direct

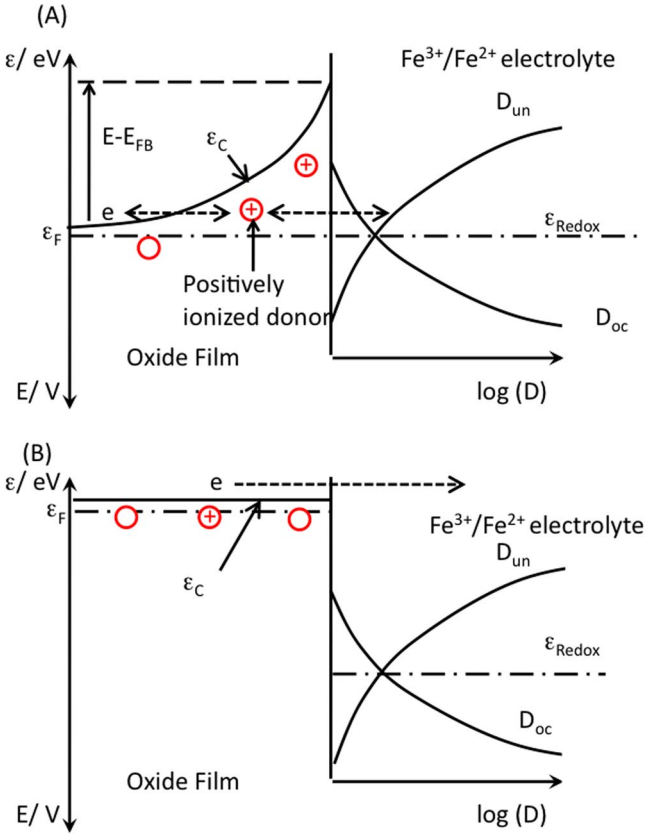

Figure 15. Relation between the conduction band edge (ε_C) and the density of state for occupied state (D_{oc}) corresponding to the state of Fe^{2+} and for unoccupied state (D_{un}) to Fe^{3+} in redox Fe^{3+}/Fe^{2+} species in the electrolyte (A) under the anodic bias at $E = E_{redox} - E_{FB}$ where E_{redox} = 0.482 V vs. SSC and E_{FB} = 0.080 V and (B) under no bias at $E = E_{FB}$ = 0.080 V. The circle (○) indicates neutral donor.

transfer from the inner side of the oxide film to the redox species in electrolyte, and the other is a route via an ionized donor site (D^+), in which the donor site works as a mediator of electron transfer.

$$e_{(CB)} + D^+ \rightleftarrows D^0$$

$$D^0 + Fe^{3+} \rightleftarrows D^+ + Fe^{2+}$$

where D^0 is a neutral donor site. In this route, the tunneling distance may be much smaller than the direct route from the inner side of the oxide to the redox species in the electrolyte, and thus the tunneling probability is much larger. The greater inhibition of electron transfer with the lower impurity concentration is explained by the lower donor density in the passive oxide film because the smaller donor density corresponds to the wider space charge layer and the fewer mediation sites.

In Fig. 15B, the potential of the steel is fixed at E_{FB} and is negatively polarized at −0.402 V against E_{Redox}.

$$E = E_{FB} = 0.080 \text{ V vs. SSC}$$

In this case, no barrier exists in the oxide film, and electrons at the conduction band edge directly transfer to the unoccupied state of Fe^{3+} and one can observe a large enough redox CD at the potential of 0.08 V, as shown in Fig. 12.

Conclusions

The properties of the passive oxide on three steels of 11Cr, 18Cr, and 30Cr-2Mo were studied in an acidic sulfate solution at pH 2.25 by

Mott-Schottky plots, potential modulation reflectance (PMR) spectroscopy, XPS measurements, and Fe^{3+}/ Fe^{2+} redox currents. For the three steels, the influence of the impurity concentration was also studied.

(1) The donor density decreased with a higher Cr content and with a lower impurity concentration.
(2) Cr enrichment took place in the passive oxide irrespective of the impurity concentration. For the 30Cr-2Mo steels, the content of Cr in the passive oxide reached approximately 70 wt%.
(3) The light absorption edge of the passive oxide measured by PMR was approximately 2.4 eV (corresponding to the wavelength at 500 nm), irrespective of the Cr content and impurity concentration.
(4) The Fe^{3+}/ Fe^{2+} redox current on the passive oxide was significantly inhibited compared with that on the Pt electrode. The redox current decreased in a similar manner to the donor density number. The inhibition of the redox current was assumed to be due to the barrier effect of the space charge layer in the n-type semiconducting passive oxide.

References

1. I. Muto, D. Ito, and N. Hara, *J. Electrochem. Soc.* **156**, C55 (2009).
2. N. Chiba, S Shibukawa, I. Muto, T. Doi, K. Kawano, Y. Sugawara, and N. Hara, *J. Electrochem. Soc.* **162**, C270 (2015).
3. N. Hara, S. Matsuda, and K. Sugimoto, *ISIJ International*, **31**, 154 (1991).
4. K. Azumi, T. Ohtsuka, and N. Sato, *J. Electrochem. Soc.*, **133**, 1326 (1986).
5. K. Azumi, T. Ohtsuka, and N. Sato, *J. Electrochem. Soc.*, **134**,1352 (1987).
6. D-S Kong, S-H. Chen, C. Wang, and W. Yang, *Corros. Sci.*, **45**, 747 (2003).
7. H. Tsuchiya, S. Fujimoto, O. Chihara, and T. Shibata, *Electrochim. Acta*, **47**, 4357 (2002).
8. E. B. Castro and J.R. Vilche, *Electrochim. Acta*, **38**, 1567 (1993).
9. K. S. Kim, J.-H. Lee, D.-K. Noh, J.-H. Kim, J. Kim, Y. Tak, and S.-H. Baeck, *Rev. Adv. Mater. Sci.* **28**, 59 (2011).
10. H. Tsuchiya, S. Fujimoto, and T. Shibata, *J. Electroceramics*, **16**, 49 (2006),
11. S. Fujimoto and H. Tsuchiya, *Corros. Sci.*, **49**, 195 (2007).
12. K. Asami, K. Hashimoto, and S. Shimodaira, *Corros. Sci.*, **18**, 151 (1978).
13. S. Fujimoto, T. Yamada, and T. Shibata, *J. Electrochem. Soc.*, **145**, L79 (1998).
14. T. Ohtsuka, A. Hyono, and Y. Sasaki, *Electrochim. Acta*, **60**, 384 (2012).
15. T. Ohtsuka, Y. Sasaki, and A. Hyono, *Electrochim. Acta*, **131**, 116 (2014).
16. K. Asami and K. Hashimoto, *Corros. Sci.*, **18**, 151 (1978).
17. C. Donic, A. Kocijan, D. Mandrino, and M. Jenko, *Metall. and Mat. Transact. B*, **42**, 1044 (2011).
18. R.-H. Jung, H. Tsuchiya, and S. Fujimoto, *Corros. Sci.*, **58**, 62 (2012).
19. U. Stimming and J. W. Schultze, *Electrochim. Acta*, **24**, 859 (1979).